GPS-observed elastic deformation due to surface mass balance variability in the Southern Antarctic Peninsula

Achraf Koulali[1], Pippa L. Whitehouse[2], Peter J. Clarke[1], Michiel R. van den Broeke[3], Grace A. Nield[2], Matt A. King[4], Michael J. Bentley[2], Bert Wouters[3,5], Terry Wilson[6]

[1]Geospatial Engineering, Newcastle University, Newcastle upon Tyne NE1 7RU, UK.
[2]Department of Geography, Durham University, South Road, Durham, DH1 3LE, UK.
[3]Institute for Marine and Atmospheric Research, Utrecht University, Utrecht, The Netherlands.
[4]School of Geography, Planning, and Spatial Sciences, University of Tasmania, Hobart, TAS, Australia.
[5]Department of Geoscience and Remote Sensing, Delft University of Technology, Delft, The Netherlands.
[6]School of Earth Sciences, Ohio State University, 125 South Oval Mall, Columbus, OH 43210-1522, USA.

Key Points:

- GPS time series of vertical deformation in the Southern Antarctic Peninsula show transient signals.
- Modelled elastic deformation due to SMB variation can largely explain these signals.
- Considering SMB elastic deformation improves estimates of linear vertical velocities.

Corresponding author: Achraf Koulali, achraf.koulali@ncl.ac.uk

This article has been accepted for publication and undergone full peer review but has not been through the copyediting, typesetting, pagination and proofreading process, which may lead to differences between this version and the Version of Record. Please cite this article as doi: 10.1029/2021GL097109.

Abstract

In Antarctica, GPS vertical time series exhibit non-linear signals over a wide range of temporal scales. To explain these non-linearities, a number of hypotheses have been proposed, among them the short-term rapid solid Earth response to contemporaneous ice mass change. Here we use GPS vertical time series to reveal the solid Earth response to variations in surface mass balance (SMB) in the Southern Antarctic Peninsula (SAP). At four locations in the SAP we show that interannual variations of SMB anomalies cause measurable elastic deformation. We use regional climate model SMB products to calculate the induced displacement assuming a perfectly elastic Earth. Our results show a reduction of the misfit when fitting a linear trend to GPS time series corrected for the elastic response to SMB variations. Our results imply that, for a better understanding of the glacial isostatic adjustment (GIA) signal in Antarctica, SMB variability must be considered.

Plain Language Summary

The Global Positioning System (GPS) allows us to measure the changing shape of the Earth's surface with high accuracy. These changes reflect multiple processes operating both within the Earth and at the surface. Using continuously recording GPS instruments in the Antarctic Peninsula, we study the response of the solid Earth to seasonal and annual variations in snow and ice accumulation over the past decade. We show that such loading triggers a measurable response that varies between years, complicating efforts to calculate the long-term Earth response to past ice sheet change. We discuss the importance of our findings for understanding feedbacks between the solid Earth and the Antarctic ice sheet.

1 Introduction

Observations of vertical land displacements from the Global Navigation Satellite System (GNSS) are now widely used to study a variety of geodynamical and climatic processes that cause solid Earth movement. Furthermore, these displacements can be used to probe the material properties of Earth's interior. For example, postseismic deformation after large earthquakes provides constraints on mantle viscosity, water content, and fault friction properties (e.g., Pollitz, 2015; Masuti et al., 2016). Similarly, ocean tide loading induced displacements have been used to infer deviations in elastic moduli relative to a reference Earth model (Ito & Simons, 2011; Bos et al., 2015; Martens et al., 2016). In polar regions, deformation in response to ice mass change provides constraints on mantle viscosity (Nield

et al., 2014; Wolstencroft et al., 2015; Zhao et al., 2017; Barletta et al., 2018; Samrat et al., 2020) and hence the strength of feedbacks between ice sheet dynamics and Earth deformation (Gomez et al., 2018).

Our understanding of the deformation caused by ice mass change in Antarctica has evolved rapidly in recent years. Thomas et al. (2011) used GPS observations to identify rapid uplift in the northern Antarctic Peninsula associated with increased ice mass loss following the Larsen B ice shelf breakup in 2002 (Rignot et al., 2008). Nield et al. (2014) extended this work and demonstrated that non-linear behaviour in the GPS time series could only be explained if the post-breakup ice loss triggered a rapid viscous, as well as an elastic, response. More recently, Barletta et al. (2018) documented higher-than-expected uplift rates (up to 41 mm/yr) in response to ice mass loss in the Amundsen Sea Embayment in West Antarctica and suggested that the response time of the mantle in that region is on the order of decades to centuries instead of thousands of years. To draw such conclusions from GPS time series requires an appreciation of the solid Earth response to both short- and long-term variations in surface mass change.

Across Antarctica, time-variable gravity changes observed from the Gravity Recovery And Climate Experiment (GRACE) mission reflect the sum contribution of contemporary ice mass change, the elastic response of the solid Earth to this contemporary change, and Earth's viscoelastic response to past ice sheet change. Isolating the signal due to past change is key to determining accurate estimates of Antarctica's current contribution to sea level. Traditionally, the signal due to past change is estimated using glacial isostatic adjustment (GIA) models (e.g., Velicogna & Wahr, 2002). Alternatively, GPS observations can provide an estimate of the GIA signal if they can be corrected for the elastic deformation signal associated with present-day ice mass change. The elastic deformation signal is usually determined by calculating the response of half-space or spherical Earth models to contemporary loads obtained from high resolution surface mass balance (SMB) models or altimetry data (e.g., Barletta et al., 2018). The latter provide time series or rates of surface height change (dh/dt) that are converted to mass trends using a density model. In most studies, the rate of mass change is considered constant throughout the time span of the GPS observation period (e.g., Wolstencroft et al., 2015). However, since elastic deformation is linearly proportional to the surface loading applied, any non-linearity in surface loading will be reflected in the elastic response.

The purpose of this study is to investigate whether elastic deformation, triggered by SMB anomalies, can explain non-linear variations in GPS vertical coordinates in the Southern Antarctic Peninsula, where there is large interannual variability of SMB and a dense network of continuous GPS stations. More generally, we investigate how different approaches to correcting for elastic effects can impact estimates of the background GIA signal, and hence our ability to better understand ice-earth feedbacks and observe linear secular vertical velocities. Martín-Español et al. (2016a) adopted an approach for deriving annually varying elastic time series from a combination of observations and models and showed clear patterns of time variability in the trends. In this study, we investigate two approaches for the calculation of the elastic deformation signal: (i) a time-dependent approach where monthly time series of elastic corrections were applied to GPS surface displacements and (ii) a static (constant-rate) approach which consists of estimating linear elastic correction rates based on surface mass trends over a specific period.

2 Data Analysis and Modelling

2.1 GPS Data

Over the Antarctic Peninsula, net surface mass balance is characterized by high spatial and temporal variability (Turner et al., 2002). For example, the three-monthly mean of the SMB anomalies from RACMO2.3 (van Wessem et al., 2018), over the Southern Antarctic Peninsula, shows a very pronounced variation in 2016 (Figure 1a,1b). The anomalies exhibit an east-west pattern suggesting a significant increase in accumulation over the western side of Palmer Land and north of the Batterbee Mountains during early summer (September – November). To investigate the surface deformation related to regional SMB variations, we considered 10 GPS sites in Palmer Land, in the Southern Antarctic Peninsula, as shown in Figure 1a. Of these, four GPS sites ran almost continuously between 2010 and late 2020 (TRVE, FOS1, JNSN and GMEZ).

We used GAMIT-GLOBK software (Herring et al., 2016) to process the GPS data in combination with a globally distributed network that includes all available data from the International GNSS Service (IGS), US POLENET-ANET and UKANET networks. We focus here on data covering the period 2010 to 2020 but the full analysis covered the period 1995 to 2020. The satellite orbit parameters were fixed to the IGS Final product values. As part of the processing, we estimated for each day the Earth orientation parameters

(EOP), station coordinates, atmospheric zenith delays and gradients at each station. We employed the time-varying a priori Zenith Hydrostatic Delay (ZHD) and Vienna Mapping function (VMF1) (Boehm et al., 2006). We corrected for the effects of ocean tide loading using the FES2004 model (Lyard et al., 2006) and we accounted for non-tidal atmospheric loading at the observation level using the European Centre for Medium-Range Weather Forecasts (ECMWF) operational analysis data (Tregoning & Watson, 2009a). Second-order ionospheric effects were accounted for using the IGS IONEX files.

We derived the coordinate time series by realizing the ITRF2014 reference frame (Altamimi et al., 2016) using a daily six-parameter transformation. We aligned our solution to the ITRF2014 using the stable approach, described in Tregoning et al. (2013), by selecting sites less affected by earthquake-related deformation (modelled displacement less than 1mm). During our processing we did not correct for non-tidal ocean loading (NTOL). However, when comparing our GPS time series with the NTOL-driven elastic deformation series obtained from the EOST/IPGS loading service (`http://loading.u-strasbg.fr`) (Mémin et al., 2020), we found that significant signals in the GPS vertical time series are not explained by NTOL (Figure S4) with only 5% WRMS reduction when subtracting the NTOL displacements from the raw GPS time series. Williams and Penna (2011) suggested that geophysical improvement of NTOL is obtained when high resolution models are used, which are not yet widely available for the Antarctic Peninsula.
Lastly, we inspected all the time series for outliers and corrected for instrumental/earthquake offsets during the velocity estimation. To estimate the linear trend from GPS time series, we used the least-squares approach with a model that includes, in addition to the linear rate, constant annual sine and cosine terms. To estimate realistic velocity uncertainties we adopted the First-Order Gauss–Markov Extrapolation (FOGMEX) algorithm (Floyd & Herring, 2019) to account for correlated noise in the time series.

The accumulation of snow/rime on GPS antennas can cause discontinuities and anomalies in the position time series (Larson, 2013). As part of the time series post-processing, we removed position outliers greater than 3-sigma with respect to the linear fit. Snow intrusion inside GPS antennas through drainage holes can also cause an apparent seasonal signal in GPS time series (Koulali & Clarke, 2020). We did not observe any change in the time series behaviour after antenna drainage holes were plugged (during the late 2016/ early 2017 field season) except at site WLCH, which shows a quasi-periodic signal that disappears after the plugging of the antenna drainage holes in December 2016. We did not attempt to correct

the WLCH time series for snow effects to avoid removing any geophysical signal that might be related to SMB. Instead, we used the approach proposed by Larson (2013) to flag and remove outliers based on the Signal-to-Noise Ratio (SNR).

2.2 Surface Mass Balance (SMB)

The mass balance (mass change) of the grounded Antarctic ice sheet depends on the trade-off between two processes: solid ice discharge across the grounding line and net surface mass accumulation, with the latter commonly referred to as surface mass balance (SMB). In ice sheet mass balance studies and also here, SMB (or, formally, the climatic mass balance; (Cogley et al., 2011)) is usually defined as the sum of surface mass gains and losses, including drifting snow processes (Lenaerts et al., 2019), and internal accumulation by refreezing of meltwater in the firn column. Understanding SMB is fundamental to understanding ice sheet contributions to global sea-level variations. In this study, we are interested in the solid Earth deformation associated with temporal and spatial SMB anomalies.

Outputs from Regional Climate Models (RCMs) are often used to estimate SMB over polar regions because they offer the possibility to investigate continent-wide temporal and spatial variability in SMB. In this study, we use the RACMO2.3p2 model (van Wessem et al., 2018), which was developed at the Royal Netherlands Meteorological Institute (KNMI) and has been adapted at Utrecht University to run over the large ice sheets of Antarctica and Greenland. Here we use the standard version of the model with 27 km spatial resolution, which covers the whole AIS, as well as the high-resolution version (5.5 km) over the Antarctic Peninsula. For comparison purposes we also use the MAR3.11 model (Kittel et al., 2018, 2021) which is available at 35 km resolution. We used monthly SMB fields across the Antarctic Ice Sheet (1979-2020), overlapping with the period of our GPS observations. Both the RACMO2 and MAR snow models are parametrized to account for the retention and refreezing of meltwater (Kittel et al., 2018). For the MAR model SMB is described as:

$$\text{SMB} = \text{precipitation} - \text{evaporation} - \text{sublimation} - \text{runoff} \tag{1}$$

The RACMO2.3p2 model includes wind-driven processes such as erosion (ERds) at the surface and sublimation (SUds) of blowing snow (Eq. 2).

$$\text{SMB} = \text{precipitation} - \text{evaporation} - \text{sublimation} - \text{runoff} - \text{SUds} - \text{ERds} \tag{2}$$

The MAR3.11 model is forced with the ERA5 reanalysis whereas the RACMO2.3 models used in this study are forced with ERA-interim (van Wessem et al., 2018). For each

model, we cumulatively summed the SMB time series and then removed the 1979-2019 trend to obtain mass anomalies with respect to the long-term linear trend. For the loading computations we converted the SMB mass anomalies into equivalent heights of a set of disc loads matching the resolution of each model, using 850 kg.m^{-3} as the density although this choice does not affect our calculated displacements (Huss, 2013). A mask (`https://www.psice.psu.edu/data/`) was defined over all the ice-shelves in the Antarctic Peninsula and loading was only applied in regions of grounded ice, including the offshore islands.

2.3 Altimetry

Separately, we used observations of ice surface elevation change (SEC), derived from a multi-mission satellite altimetry dataset (Schröder et al., 2019), to construct an independent time series of surface mass change across Antarctica. We defined a loading model using monthly grids of surface elevation change and assuming an ice density of 850 kg.m^{-3}. Each grid reflects the change in surface elevation since the reference epoch of 09/2010 and has a spatial resolution of 10 km. Our loading history covers the time period between 09/2010 and 12/2017. Surface elevation change, as observed by altimetry, can be the result of SMB changes, compaction of the firn column, or dynamic thinning or thickening due to changes in ice flow speed (neglecting basal melt). We use altimetry SEC data here only for independent validation of the signal we observe in GPS time series and discuss below how we deal with firn densification, which takes place in the absence of net mass change. We do not attempt to isolate the ice-dynamic component from the SMB signal, and we assume that its temporal variation is smooth compared to SMB (Martín-Español et al., 2016a).

2.4 Elastic deformation modelling

We consider deformation due to annual and interannual fluctuations of SMB to be purely elastic in this region. This is supported by past GPS studies that suggest the viscosity of the upper mantle in this region is likely $> 10^{20}$ Pa.s (Zhao et al., 2017; Wolstencroft et al., 2015) in contrast to the very low viscosities inferred for the northern AP ($0.3-3\times10^{18}$ Pa.s) (Nield et al., 2014; Samrat et al., 2020, 2021).

We modelled the vertical surface displacements caused by SMB loading using the Regional ElAstic Rebound calculator REAR (Melini et al., 2015). The Green's functions were

spatially convolved with the SMB loading. Load Love numbers were computed in the center-of-figure (CF) frame (Blewitt, 2003) up to degree 10000 (equivalent to a half wavelength of 2.25 km). We adopted the Preliminary Reference Earth Model (PREM; Dziewonski and Anderson (1981)). Following Martens et al. (2016) we defined a waterless crustal structure with Vp=5800 m.s^{-1}, Vs=3200 m.s^{-1} and density=2600 kg.m^{-3}. We assumed the same ice density as was used to convert SMB anomalies to heights. Here, by using the PREM model we do not consider the effects of lateral heterogeneity of the Earth's structure. We assume that the elastic parameters do not show wide variations within our study region. Dill et al. (2015) found that Green's functions vary by about 12% in the vertical component at a distance of 0.25°.

2.4.1 Time series approach

The monthly surface mass loads derived from the SMB models and the altimetry SEC (described in sections 2.2 and 2.3) were convolved with surface load Green's functions. The resulting surface deformation time series were interpolated into daily series using a cubic spline. Thus, for each GPS site we derived an elastic time series that was used to correct the observed position time series before estimating long-term linear rates. Figure 1c,1f shows de-trended GPS time series and modelled vertical displacement at the four GPS sites with the most complete observations during the 2016-2017 seasons.

2.4.2 Linear rates approach

Linear velocities estimated from GPS time series are often (e.g., Thomas et al., 2011; Wolstencroft et al., 2015) corrected for the response to contemporary surface mass change using linear trends of elastic corrections over a given period. As mentioned before, this approach assumes that the SMB loading trend is constant in time. To gain insight on how this approach compares to our time series approach, we modelled the linear rate of elastic deformation over three periods: 2010-2014, 2014-2017 and 2010-2017 using the 10 km gridded SEC altimetry product of Schröder et al. (2019). To remove the signal due to firn densification we use the firn densification model (FDM) that is provided with RACMO2.3 (Ligtenberg et al., 2011). Following Wolstencroft et al. (2015), we performed a Monte Carlo simulation and generated 500 realisations of the surface mass change rate while propagating the uncertainties in the various data products: for each simulation, we sampled the uncertainties provided with the altimetry elevation change product and the FDM model, and we

considered a 20% error in the SMB change estimates (Wouters et al., 2015). The mean trend of the ensemble was used to calculate the linear elastic deformation rate, and the standard deviation was used to define uncertainties on the elastic rates, which were then propagated into the GPS-estimated linear vertical velocities.

3 Results and Discussion

We compare de-trended GPS time series with elastic deformation time series calculated using three SMB models and find that the SMB-forced elastic deformation predictions closely reproduce the main features of the observed vertical displacement variations (Figure 1). The three SMB-forced elastic deformation models show an overall comparable fit to the GPS time series, although the RACMO2.3 (5.5 km) model better fits the GPS signal between 2010 and 2012. For example, we obtain a Spearman's rank correlation coefficient of 0.78 between the observed TRVE GPS time series and the RACMO2.3 (5.5 km) derived elastic deformation, compared with 0.76 for RACMO2.3 (27 km) and 0.75 for MAR3.11 (35 km). This suggests that the high-resolution SMB model better resolves small-scale, topographically forced SMB gradients, thus allowing the recovery of finer short wavelength deformation (van Wessem et al., 2018).

3.1 SMB elastic deformation

The most striking feature in the GPS time series of the four sites is the subsidence signal observed between early 2016 and early 2017: we observed between 11 and 20 mm subsidence within 7 months, in agreement with the pattern in Figure 1a,1b, which shows an increase in SMB anomalies during 2016. This short-term variability is in line with the results of Thomas et al. (2008) who documented high interannual accumulation variability in West Antarctica during the 20^{th} century. Additionally, spectral analysis of Antarctic SMB time series from RACMO and ice cores shows that the highest power is at the lowest frequencies (King & Watson, 2020), which reflects the contribution of a stochastic annual and interannual variability in SMB time series. The magnitude of the variations recorded in the GPS time series is variable from site to site, which likely relates to the geographic location of each site with respect to the topographic features controlling accumulation patterns in the SAP (Kaspari et al., 2004).

We subtracted the calculated elastic deformation using the time series approach (section 2.4.1) from all 10 GPS coordinate time series and calculated the weighted root mean square (WRMS) of the detrended residuals (Figure 2a). We clearly observe an improvement after correcting for SMB effects compared with the raw time series. The median WRMS reduction for all the sites in our study is 23% for RACMO2.3 (5.5 km), 21% for MAR3.11 and 17% for RACMO2.3 (27 km). The ability of the RACMO2.3 (5.5 km) model to better resolve topographic contrasts in the SAP allows a better simulation of the strong spatial SMB gradients, in turn resulting in better resolved temporal loading variations (van Wessem et al., 2016; van Wessem et al., 2018). This agrees with Mottram et al. (2020) who showed that the gain of increasing spatial resolution in SMB models is mostly seen in regions with complex topography such as the SAP.

The highest reduction in the WRMS occurs for the RACMO2.3 high resolution (5.5 km) model at almost all sites, except for GMEZ and BREN which show approximately similar WRMS between the three SMB models. BREN has very extended gaps of missing observations and therefore results for this site should be treated with caution (Figure S2). At some sites, the greatest WRMS reduction is achieved when using the SEC approach (Figure 2a). This may reflect the fact that the observation-based SEC approach better represents the load history compared with the SMB re-analysis products. However, differences may also be due to the fact that the SEC results are calculated over a slightly shorter time period.

It is well known that non-stationary signals in GPS time series can distort estimates of long-term secular linear rates (e.g., Tregoning et al., 2009b). Santamaría-Gómez and Mémin (2015) found that, globally, the response to interannual surface load variations cannot be considered white or time-uncorrelated, but is better characterized by a power-law process, suggesting that a decade of continuous data is required to mitigate the impact of such variations on the estimation of secular velocities. It follows that not accounting for elastic deformation due to contemporary SMB variability may result in biased linear uplift estimates.

As we have shown in this study, elastic deformation due to contemporary SMB variability is highly time dependent and varies between GPS sites. In Figure 2b we compare linear GPS velocities corrected for contemporaneous elastic deformation using a linear approach (section 2.4.2) with velocities derived after correcting the GPS time series for time-varying elastic deformation (Table S1), where the RACMO 2.3 (5.5km) model is used to determine

the elastic time series correction. Figure 2b shows that velocities corrected using linear elastic rates over 2010-2014 differ from those using linear elastic rates over 2014-2017 or 2010-2017. This is a result of the large magnitude, time-dependent nature of surface mass change. The time series approach does not require any assumption of linearity over the observation period, providing a more robust way of isolating the secular linear trend in GPS observations, which can then be associated with GIA. Martín-Español et al. (2016a) proposed a more integrated approach using a Bayesian framework, which inverts GPS, altimetry, and gravity data to resolve the different components contributing to surface elevation changes. Similar to our findings, they showed that elastic deformation varies over time across the SAP, shifting from subsidence during the period 2003-2009 to uplift during the period 2010-2013.

3.2 Implication for vertical land motion rates

In Figure 3 we show a comparison between four model predictions of present-day GIA-related uplift rates and the estimated GPS rates after correction using the time series approach. We selected three forward GIA models widely used in the literature: W12a (Whitehouse et al., 2012), ICE_6G_D (Peltier et al., 2018) and IRJ05_R2 (Ivins et al., 2013) as well as a data-driven model: Gunter2014 (CSR RL05 DDK5) (Gunter et al., 2014), which is based on the Release-05 GRACE solution from the Center for Space Research (CSR) and is not constrained with GPS observations. The three forward models show significant variation in terms of the magnitude and pattern of uplift over the study area, which reflects differences in the deglaciation history as well as the choice of rheological Earth model.

The solution of Gunter2014 is the closest to the GPS observations, with a WRMS of 0.95 mm/yr, as also found with a briefer time series by Wolstencroft et al. (2015). Although this model reproduces well the pattern of deformation at most sites, a disagreement is seen at sites FOS1 and WLCH, where the GPS observes subsidence rates of -0.95 ± 0.26 mm/yr and -0.76 ± 0.13 mm/y, respectively, whereas the model predicts an uplift of 0.41 mm/yr for FOS1 and 0.61 mm/yr for WLCH. Comparing the GPS observations with the W12a model prediction yields a WRMS of 3.11 mm/yr compared with WRMS of 2.24 and 2.04 mm/yr for the ICE_6G_D and IRJ05_R2 models, respectively. W12a predicts a region of subsidence surrounded by uplift. A similar pattern is observed by the GPS but the locations of observed and modelled subsidence are offset, leading to misfits at JNSN, BREN, HTON and GMEZ. We should mention here that the GPS antenna of site BREN

was replaced twice since its installation in 2006 (in 2012 and 2014), thus a longer time span of observations is needed to robustly constrain vertical uplift at this location. We did not consider the difference in the centre-of-mass reference frame between GPS secular velocities and GIA model predictions (Argus et al., 2014), nor the effects of signals due to far-field (non-Antarctic) elastic deformation (e.g., Frederikse et al., 2017). These effects are small and likely to be less than 0.5mm/yr (Sun & Riva, 2020).

The models ICE_6G_D and IRJ05_R2 also show significant disagreement with the uplift observations and, reflecting the findings of Martín-Español et al. (2016b), they both over-predict the GIA signal compared with the GPS observations. The ICE_6G_D model was tuned based on comparison with the GPS rates available at the time. However, as we have shown in this study, the background linear rate derived from GPS time series depends on how well we can model the present-day elastic deformation, hence caution should be applied when tuning GIA models using observations that contain multiple signals.

4 Conclusion

We use continuous GPS time series from the Southern Antarctic Peninsula in combination with SMB models to investigate the existence of an elastic signal associated with interannual SMB variations within vertical component positions between 2010 and 2020. We demonstrate that GPS vertical displacement time series contain time-varying elastic signals due to SMB variations. Our comparison between GPS time series and elastic deformation calculated using SMB models shows good agreement and a reduction of the WRMS of the residuals. We find that the elastic deformation derived from the high resolution SMB model RACMO2.3 (5.5 km) is in better agreement with the GPS observations than RACMO2.3 (27 km) and MAR3.11 (35 km), perhaps due to the high sensitivity of accumulation patterns to local topography. Correcting GPS time series for SMB-related deformation using a time series approach provides consistent estimates of long-term vertical land motion rates.

Given that GPS time series include a range of transient non-linear signals, their interpretation by simply fitting standard linear trajectory models is prone to biases in both the estimates and in the uncertainties derived from noise around a linear model. It is therefore imperative to understand and model the sources of short-term variations such as the SMB-related deformations studied here.

Despite large differences between the GPS observations and the GIA models considered here, we show patterns of similarity. Our GPS-derived vertical rates are in closer agreement with the inverse GIA solution of Gunter et al. (2014) than conventional GIA forward models, as also found by Martín-Español et al. (2016b). This likely reflects the fact that current GIA forward models do not account for recent, centennial-scale ice sheet changes (e.g., Nield et al., 2012) that will contribute to the contemporary GIA signal. Further improvements in GPS data processing and reference frame realization, and quantification of SMB variations, will allow us to better identify the solid Earth response to contemporary surface mass change and hence isolate the GIA signal.

In this study, we have modelled short-term variations in surface deformation using a purely elastic model. However, a more complete description of SMB-related deformation should include the mantle response at longer time scales by considering viscoelastic models. Our results suggest that recovery of the background response of the solid Earth to long-term Antarctic Ice Sheet change depends on our ability to model present-day non-linear signals recorded in GPS observations.

Open Research

GPS data used in this study are from the UKANET network and are available through UNAVCO at `https://www.unavco.org/data/dai`. Data identifiers are available at `https://www.unavco.org/data/doi/10.7283/T56Q1VN5`. GPS time series used in this study are available in the Zenodo repository `https://doi.org/10.5281/zenodo.5939016`. Time series of modeled Non-tidal ocean loading displacements (Figure S4) are from the EOST loading service `http://loading.u-strasbg.fr`.

Acknowledgments

We thank David Maxfield, Paul Breen, Thomas Nylen, and other personnel from the British Antarctic Survey (BAS) and UNAVCO for support with data acquisition and network management. The GPS data processing was performed on the Rocket High Performance Computing service at Newcastle University. This work is supported by the UK Natural Environment Research Council (NERC) grant NE/R002029/1. AK was partially supported by the NERC grant NE/K004085/1. MRvdB acknowledges support from the Netherlands Earth System Science Centre (NESSC). BW was supported by NWO VIDI grant 016.Vidi.171.063.

We are grateful to the two reviewers whose careful and constructive comments helped improve the paper.

References

Altamimi, Z., Rebischung, P., Métivier, L., & Collilieux, X. (2016). ITRF2014: A new release of the international terrestrial reference frame modeling nonlinear station motions. *Journal of Geophysical Research: Solid Earth*, *121*(8), 6109–6131.

Argus, D. F., Peltier, W., Drummond, R., & Moore, A. W. (2014). The Antarctica component of postglacial rebound model ICE-6G_C (VM5a) based on gps positioning, exposure age dating of ice thicknesses, and relative sea level histories. *Geophysical Journal International*, *198*(1), 537–563.

Barletta, V. R., Bevis, M., Smith, B. E., Wilson, T., Brown, A., Bordoni, A., ... others (2018). Observed rapid bedrock uplift in amundsen sea embayment promotes ice-sheet stability. *Science*, *360*(6395), 1335–1339.

Blewitt, G. (2003). Self-consistency in reference frames, geocenter definition, and surface loading of the solid earth. *Journal of geophysical research: solid earth*, *108*(B2).

Boehm, J., Werl, B., & Schuh, H. (2006). Troposphere mapping functions for GPS and very long baseline interferometry from european centre for medium-range weather forecasts operational analysis data. *Journal of geophysical research: solid earth*, *111*(B2).

Bos, M. S., Penna, N. T., Baker, T. F., & Clarke, P. J. (2015). Ocean tide loading displacements in western europe: 2. GPS-observed anelastic dispersion in the asthenosphere. *Journal of Geophysical Research: Solid Earth*, *120*(9), 6540–6557.

Cogley, J. G., Hock, R., Rasmussen, L., Arendt, A., Bauder, A., Braithwaite, R., ... others (2011). Glossary of glacier mass balance and related terms. *IHP-VII technical documents in hydrology*, *86*.

Dill, R., Klemann, V., Martinec, Z., & Tesauro, M. (2015). Applying local green's functions to study the influence of the crustal structure on hydrological loading displacements. *Journal of Geodynamics*, *88*, 14–22.

Dziewonski, A. M., & Anderson, D. L. (1981). Preliminary reference earth model. *Physics of the earth and planetary interiors*, *25*(4), 297–356.

Floyd, M. A., & Herring, T. A. (2019). Fast statistical approaches to geodetic time series analysis. *Geodetic Time Series Analysis in Earth Sciences Bos and Montillet, Springer Geophysics. Cham: Springer. https://doi. org/10.1007/978-3-030-21718-1*.

Frederikse, T., Riva, R. E., & King, M. A. (2017). Ocean bottom deformation due to present-day mass redistribution and its impact on sea level observations. *Geophysical Research Letters*, *44*(24), 12–306.

Gomez, N., Latychev, K., & Pollard, D. (2018). A coupled ice sheet–sea level model incorporating 3d earth structure: variations in Antarctica during the last deglacial retreat. *Journal of Climate*, *31*(10), 4041–4054.

Gunter, B., Didova, O., Riva, R., Ligtenberg, S., Lenaerts, J., King, M., ... Urban, T. (2014). Empirical estimation of present-day antarctic glacial isostatic adjustment and ice mass change. *The Cryosphere*, *8*(2), 743–760.

Herring, T. A., Melbourne, T. I., Murray, M. H., Floyd, M. A., Szeliga, W. M., King, R. W., ... Wang, L. (2016). Plate boundary observatory and related networks: GPS data analysis methods and geodetic products. *Reviews of Geophysics*, *54*(4), 759–808.

Huss, M. (2013). Density assumptions for converting geodetic glacier volume change to mass change. *The Cryosphere*, *7*(3), 877–887.

Ito, T., & Simons, M. (2011). Probing asthenospheric density, temperature, and elastic moduli below the western united states. *Science*, *332*(6032), 947–951.

Ivins, E. R., James, T. S., Wahr, J., O. Schrama, E. J., Landerer, F. W., & Simon, K. M. (2013). Antarctic contribution to sea level rise observed by GRACE with improved GIA correction. *Journal of Geophysical Research: Solid Earth*, *118*(6), 3126–3141.

Kaspari, S., Mayewski, P. A., Dixon, D. A., Spikes, V. B., Sneed, S. B., Handley, M. J., & Hamilton, G. S. (2004). Climate variability in west Antarctica derived from annual accumulation-rate records from ITASE firn/ice cores. *Annals of Glaciology*, *39*, 585–594.

King, M. A., & Watson, C. S. (2020). Antarctic surface mass balance: Natural variability, noise, and detecting new trends. *Geophysical Research Letters*, *47*(12), e2020GL087493.

Kittel, C., Amory, C., Agosta, C., Delhasse, A., Doutreloup, S., Huot, P.-V., ... Fettweis, X. (2018). Sensitivity of the current antarctic surface mass balance to sea surface conditions using MAR. *The Cryosphere*, *12*(12), 3827–3839.

Kittel, C., Amory, C., Agosta, C., Jourdain, N. C., Hofer, S., Delhasse, A., ... others (2021). Diverging future surface mass balance between the antarctic ice shelves and grounded ice sheet. *Cryosphere*, *15*(3), 1215–1236.

Koulali, A., & Clarke, P. (2020). Effect of antenna snow intrusion on vertical GPS position

time series in Antarctica. *Journal of Geodesy*, *94*(10), 1–11.

Larson, K. M. (2013). A methodology to eliminate snow-and ice-contaminated solutions from GPS coordinate time series. *Journal of Geophysical Research: Solid Earth*, *118*(8), 4503–4510.

Lenaerts, J. T., Medley, B., van den Broeke, M. R., & Wouters, B. (2019). Observing and modeling ice sheet surface mass balance. *Reviews of Geophysics*, *57*(2), 376–420.

Ligtenberg, S., Helsen, M., & Van den Broeke, M. (2011). An improved semi-empirical model for the densification of antarctic firn. *The Cryosphere*, *5*(4), 809–819.

Lyard, F., Lefévre, F., Letellier, T., & Francis, O. (2006). Modelling the global ocean tides: modern insights from FES2004. *Ocean dynamics*, *56*(5-6), 394–415.

Martens, H. R., Rivera, L., Simons, M., & Ito, T. (2016). The sensitivity of surface mass loading displacement response to perturbations in the elastic structure of the crust and mantle. *Journal of Geophysical Research: Solid Earth*, *121*(5), 3911–3938.

Martín-Español, A., King, M. A., Zammit-Mangion, A., Andrews, S. B., Moore, P., & Bamber, J. L. (2016b). An assessment of forward and inverse GIA solutions for Antarctica. *Journal of Geophysical Research: Solid Earth*, *121*(9), 6947–6965.

Martín-Español, A., Zammit-Mangion, A., Clarke, P. J., Flament, T., Helm, V., King, M. A., ... others (2016a). Spatial and temporal antarctic ice sheet mass trends, glacio-isostatic adjustment, and surface processes from a joint inversion of satellite altimeter, gravity, and GPS data. *Journal of Geophysical Research: Earth Surface*, *121*(2), 182–200.

Masuti, S., Barbot, S. D., Karato, S.-i., Feng, L., & Banerjee, P. (2016). Upper-mantle water stratification inferred from observations of the 2012 indian ocean earthquake. *Nature*, *538*(7625), 373–377.

Melini, D., Gegout, P., Midi-Pyrenees, O., & Spada, G. (2015). A regional elastic rebound calculator.

Mémin, A., Boy, J.-P., & Santamaria-Gomez, A. (2020). Correcting gps measurements for non-tidal loading. *GPS Solutions*, *24*(2), 1–13.

Menemenlis, D., Campin, J.-M., Heimbach, P., Hill, C., Lee, T., Nguyen, A., ... Zhang, H. (2008). Ecco2: High resolution global ocean and sea ice data synthesis. *Mercator Ocean Quarterly Newsletter*, *31*(October), 13–21.

Mottram, R., Hansen, N., Kittel, C., van Wessem, M., Agosta, C., Amory, C., ... others (2020). What is the surface mass balance of Antarctica? an intercomparison of regional

climate model estimates. *The Cryosphere Discussions*, 1–42.

Nield, G. A., Barletta, V. R., Bordoni, A., King, M. A., Whitehouse, P. L., Clarke, P. J., ... Berthier, E. (2014). Rapid bedrock uplift in the antarctic peninsula explained by viscoelastic response to recent ice unloading. *Earth and Planetary Science Letters*, *397*, 32–41.

Nield, G. A., Whitehouse, P. L., King, M. A., Clarke, P. J., & Bentley, M. J. (2012). Increased ice loading in the antarctic peninsula since the 1850s and its effect on glacial isostatic adjustment. *Geophysical Research Letters*, *39*(17).

Peltier, R. W., Argus, D. F., & Drummond, R. (2018). Comment on "an assessment of the ICE-6G_C (VM5a) glacial isostatic adjustment model" by purcell et al. *Journal of Geophysical Research: Solid Earth*, *123*(2), 2019–2028.

Pollitz, F. F. (2015). Postearthquake relaxation evidence for laterally variable viscoelastic structure and water content in the southern california mantle. *Journal of Geophysical Research: Solid Earth*, *120*(4), 2672–2696.

Rignot, E., Bamber, J. L., Van Den Broeke, M. R., Davis, C., Li, Y., Van De Berg, W. J., & Van Meijgaard, E. (2008). Recent antarctic ice mass loss from radar interferometry and regional climate modelling. *Nature geoscience*, *1*(2), 106–110.

Samrat, N. H., King, M. A., Watson, C., Hay, A., Barletta, V., & Bordoni, A. (2021). Upper mantle viscosity underneath northern marguerite bay, antarctic peninsula constrained by bedrock uplift and ice mass variability. *Geophysical Research Letters*, e2021GL097065.

Samrat, N. H., King, M. A., Watson, C., Hooper, A., Chen, X., Barletta, V. R., & Bordoni, A. (2020). Reduced ice mass loss and three-dimensional viscoelastic deformation in northern antarctic peninsula inferred from GPS. *Geophysical Journal International*, *222*(2), 1013–1022.

Santamaría-Gómez, A., & Mémin, A. (2015). Geodetic secular velocity errors due to interannual surface loading deformation. *Geophysical Journal International*, *202*(2), 763–767.

Schröder, L., Horwath, M., Dietrich, R., Helm, V., Broeke, M. R., & Ligtenberg, S. R. (2019). Four decades of antarctic surface elevation changes from multi-mission satellite altimetry. *The Cryosphere*, *13*(2), 427–449.

Sun, Y., & Riva, R. E. (2020). A global semi-empirical glacial isostatic adjustment (GIA) model based on gravity recovery and climate experiment (GRACE) data. *Earth System*

Dynamics, *11*(1), 129–137.

Thomas, E. R., Marshall, G. J., & McConnell, J. R. (2008). A doubling in snow accumulation in the western antarctic peninsula since 1850. *Geophysical research letters*, *35*(1).

Thomas, I. D., King, M. A., Bentley, M. J., Whitehouse, P. L., Penna, N. T., Williams, S. D., ... others (2011). Widespread low rates of antarctic glacial isostatic adjustment revealed by GPS observations. *Geophysical Research Letters*, *38*(22).

Tregoning, P., Burgette, R., McClusky, S., Lejeune, S., Watson, C. S., & McQueen, H. (2013). A decade of horizontal deformation from great earthquakes. *Journal of Geophysical Research: Solid Earth*, *118*(5), 2371–2381.

Tregoning, P., Ramillien, G., McQueen, H., & Zwartz, D. (2009b). Glacial isostatic adjustment and nonstationary signals observed by GRACE. *Journal of Geophysical Research: Solid Earth*, *114*(B6).

Tregoning, P., & Watson, C. (2009a). Atmospheric effects and spurious signals in GPS analyses. *Journal of Geophysical Research: Solid Earth*, *114*(B9).

Turner, J., Lachlan-Cope, T., Marshall, G., Morris, E., Mulvaney, R., & Winter, W. (2002). Spatial variability of antarctic peninsula net surface mass balance. *Journal of Geophysical Research: Atmospheres*, *107*(D13), AAC–4.

van Wessem, J. M., Ligtenberg, S. R. M., Reijmer, C. H., van de Berg, W. J., van den Broeke, M. R., Barrand, N. E., ... van Meijgaard, E. (2016). The modelled surface mass balance of the antarctic peninsula at 5.5 km horizontal resolution. *The Cryosphere*, *10*(1), 271–285.

van Wessem, J. M., van de Berg, W. J., Noël, B. P. Y., van Meijgaard, E., Amory, C., Birnbaum, G., ... van den Broeke, M. R. (2018). Modelling the climate and surface mass balance of polar ice sheets using RACMO2–part 2: Antarctica (1979–2016). *The Cryosphere*, *12*(4), 1479–1498.

Velicogna, I., & Wahr, J. (2002). A method for separating antarctic postglacial rebound and ice mass balance using future icesat geoscience laser altimeter system, gravity recovery and climate experiment, and gps satellite data. *Journal of Geophysical Research: Solid Earth*, *107*(B10), ETG–20.

Whitehouse, P. L., Bentley, M. J., Milne, G. A., King, M. A., & Thomas, I. D. (2012). A new glacial isostatic adjustment model for Antarctica: calibrated and tested using observations of relative sea-level change and present-day uplift rates. *Geophysical Journal International*, *190*(3), 1464–1482.

Williams, S., & Penna, N. (2011). Non-tidal ocean loading effects on geodetic gps heights. *Geophysical Research Letters*, *38*(9).

Wolstencroft, M., King, M. A., Whitehouse, P. L., Bentley, M. J., Nield, G. A., King, E. C., ... others (2015). Uplift rates from a new high-density GPS network in palmer land indicate significant late holocene ice loss in the southwestern weddell sea. *Geophysical Journal International*, *203*(1), 737–754.

Wouters, B., Martin-Español, A., Helm, V., Flament, T., van Wessem, J. M., Ligtenberg, S. R., ... Bamber, J. L. (2015). Dynamic thinning of glaciers on the southern antarctic peninsula. *Science*, *348*(6237), 899–903.

Zhao, C., King, M. A., Watson, C. S., Barletta, V. R., Bordoni, A., Dell, M., & Whitehouse, P. L. (2017). Rapid ice unloading in the fleming glacier region, southern antarctic peninsula, and its effect on bedrock uplift rates. *Earth and Planetary Science Letters*, *473*, 164–176.

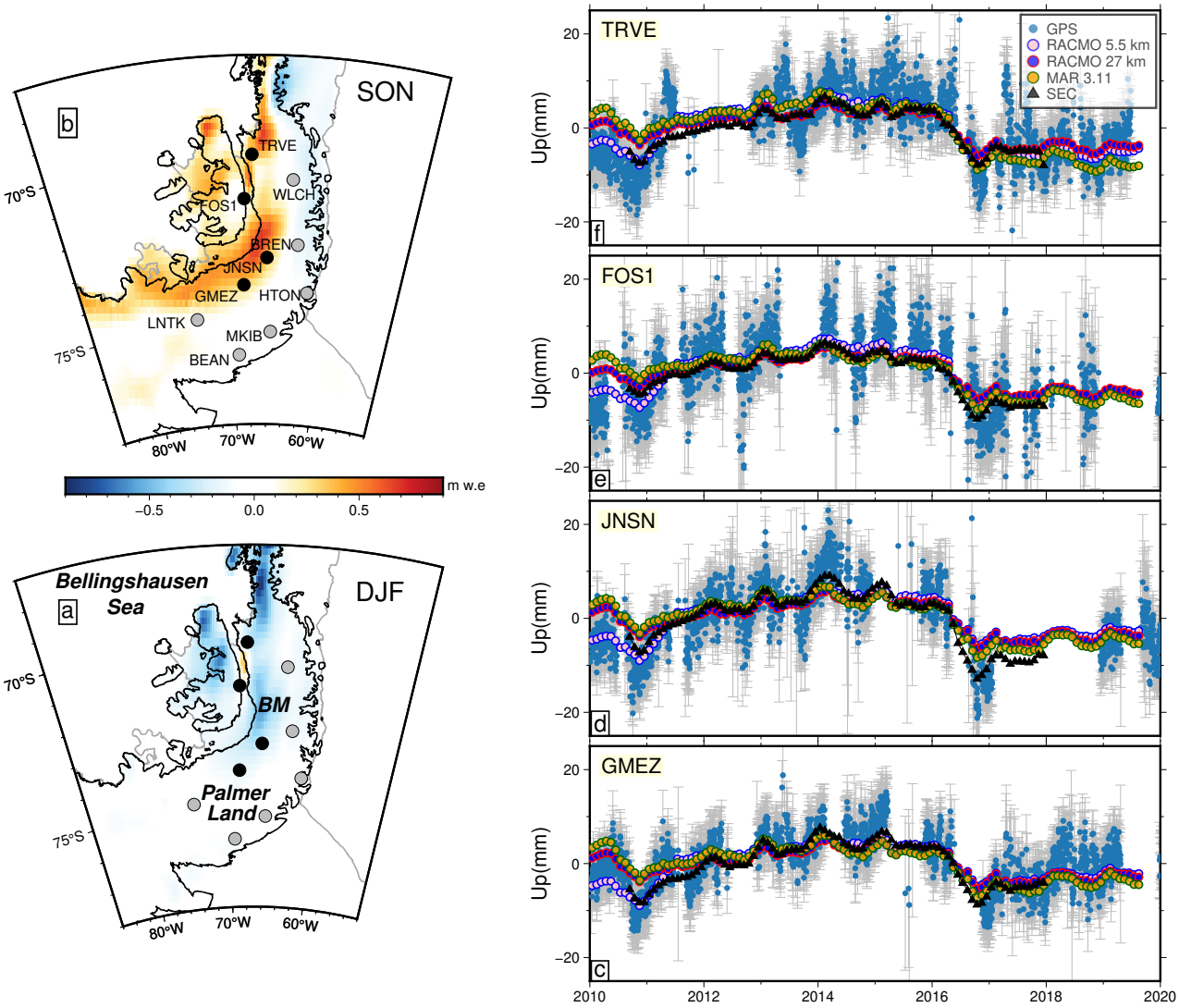

Figure 1. (a-b) Three-monthly mean DJF (December 2015 - February 2016) and SON (September - November 2016) of the surface mass balance anomaly with respect to the linear trend (1979-2019) from the RACMO2.3 (27km) model. The continuous black line is the ice sheet grounding line, grey lines denote ice shelf boundaries. Dots indicate the locations of GPS sites. Black dots are the sites used in subplots c,d,e,f. BM: Batterbee Mountains. (c,d,e,f) Daily de-trended vertical GPS time series (blue dots, with one standard deviation error bars in grey) and elastic deformation computed from monthly SMB anomalies with respect to the linear trend (1979-2019), and the altimetry Surface Elevation Change (SEC) product of Schröder et al. (2019) between September-2010 and December-2017.

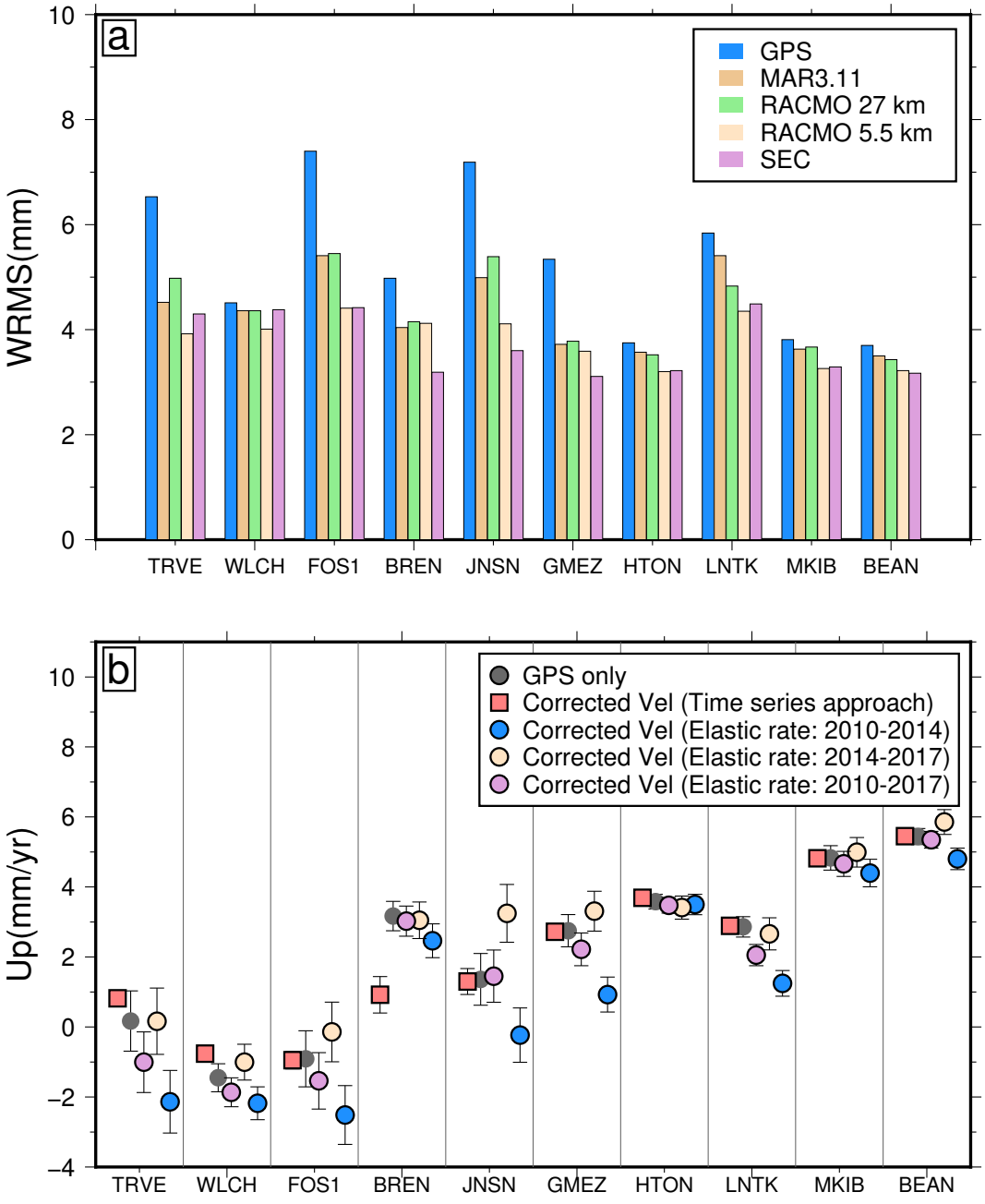

Figure 2. (a) WRMS residuals to the fit of a linear trend to the raw GPS time series (blue) and to GPS time series after subtraction of elastic deformation time series due to SMB anomalies. (b) GPS linear vertical velocities estimated from the raw position time series (black) as well as after correction for present-day elastic deformation due to mass change using the "linear" (green, orange and blue circles) and the "time series" (magenta squares) approach using the RACMO2.3 (5.5 km resolution) model. Error bars reflect 95% confidence intervals.

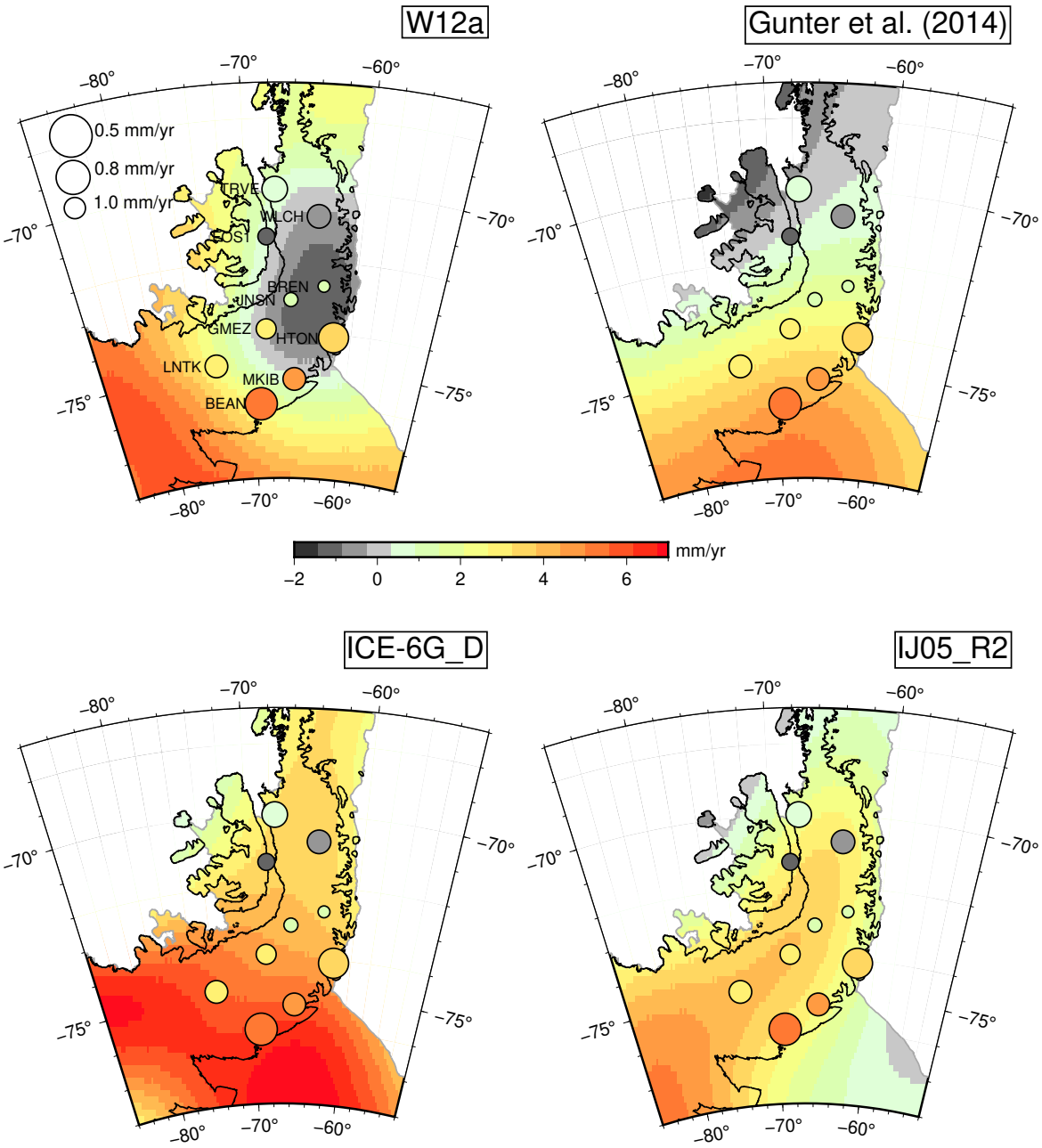

Figure 3. Vertical displacement rates from published GIA models and estimated from GPS time series corrected for elastic deformation using RACMO2.3 (5.5 km resolution). The colour of the circles represents the vertical velocity and their size represents the 95% confidence interval uncertainty.